

# Underwater Image Color Correction by Complementary Adaptation

Yuchen He

## Abstract

In this paper, we propose a novel approach for underwater image color correction based on a Tikhonov type optimization model in the CIELAB color space. It presents a new variational interpretation of the complementary adaptation theory in psychophysics, which establishes the connection between colorimetric notions and color constancy of the human visual system (HVS). Understood as a long-term adaptive process, our method effectively removes the underwater color cast and yields a balanced color distribution. For visualization purposes, we enhance the image contrast by properly rescaling both lightness and chroma without trespassing the CIELAB gamut. The magnitude of the enhancement is hue-selective and image-based, thus our method is robust for different underwater imaging environments. To improve the uniformity of CIELAB, we include an approximate hue-linearization as the pre-processing and an inverse transform of the Helmholtz-Kohlrausch effect as the post-processing. We analyze and validate the proposed model by various numerical experiments. Based on image quality metrics designed for underwater conditions, we compare with some state-of-art approaches to show that the proposed method has consistently superior performances.

## 1 Introduction

Water absorbs light similarly to an optical filter but with higher variations and complexities [43]. Depending on the dissolved or suspended substances, a liquid medium modifies the spectral power distribution of the transmitted light, such that a strong bluish or greenish color cast dominates the acquired underwater image, e.g., Figure 1 (Top). Typically, underwater images have insufficient contrast and unbalanced color distribution [4, 31, 40, 42, 43], hence many image contents, such as patterns and textures are hardly recognizable for human observers. An effective color correction method is needed to recover and enhance these details.

We can understand this task as reversing the process of image formation. The complex factors determining the irradiance on an imaging sensor are often simplified by the Koschmieder model [19]. It expresses the image colors as a convex combination of the unattenuated objects' colors and the veiling light via a scalar transmission map. The veiling light is approximated by various types of dark-channel priors [31, 40, 42], and the estimation of the transmission map is converted to depth computation based on the Beer-Lambert law [36]. Hence, for any combination of a veiling light and a transmission map, the color-corrected image is uniquely determined. These methods are sensitive to the identified veiling lights such that small perturbations on the estimated RGB values of the background trigger visually significant results [31]. More sophisticated models along this direction consider the Jerlov's water types [4, 17] to improve the stability.

Essentially, we are finding a color distribution on the image domain that is favorable for a human observer. Different from models of physics, many methods in the literature adjust the image colors based on principles of the human visual system (HVS). One of the important properties of HVS is color constancy: the appearance of the color of an object remains approximately stable under varying illuminations [2]. This chromatic adaptation for instance allows an



Figure 1: (Top) Underwater image with heavy green cast. (Bottom) Result of the proposed method. In the middle, several zoomed-in regions are displayed for comparison. The resulted image has enhanced contrast, balanced colors, and many image contents, e.g., the patterns on the swimming shorts, are more recognizable. In this paper, all the underwater images are from the benchmark data set [21].



observer to recognize the brown statue and the blue shorts in Figure 1 (Top), even though the image is dominated by a heavy green cast. Theories [12, 13, 26] have been proposed to explain the underlying mechanism from various perspectives including the well-known Retinex theory by Land [20]. It is argued that HVS perceives a scene based on local variation of image lightness rather than an absolute lightness, and this theory induces a huge class of algorithmic interpretations of the adaptation process applied in computer vision, e.g., Multiscale Retinex [32, 34], random-spray Retinex [33], non-local Retinex [45] and many others [18, 27, 28].

In this paper, we propose a novel approach for underwater image color correction which converts Figure 1 (Top) to (Bottom), whose color distribution is more balanced and compatible with HVS. Instead of the Retinex theory, we present a new mathematical interpretation for the Complementary Adaptation Theory (CAT) first formulated by Gibson [15] in 1937. The key principle is that, the quality of a constantly applied stimulus will be temporarily shifted towards the corresponding complementary quality, thus resulting in a neutral state. This applies not only to HVS, but also to other bilateral sensory processes, e.g., temperature perception. Both Retinex theory and CAT emphasize the importance of relative levels over absolute levels of sensation, yet they are fundamentally different in the following aspects.

- *Mechanism*: The Retinex theory ascribes the color constancy to HVS’s ability of estimating the reflectance independent from the illumination, while CAT describes the color constancy as a result from the neutralization of the illumination by a negative sensory process.
- *Role of illuminating color*: In Retinex theory, illumination is treated as unknown and its color can be derived after identifying the reflectance; whereas in CAT, the illuminating light determines the direction and magnitude of the adaptation process.
- *Adapting time*: The Retinex theory was supported by experiments with short-time adapting; in contrast, recent experiments show that the chromatic neutralization predicted by CAT occurs after multiple days [3, 38].

Our method captures these features of CAT and produces a color distribution complying with the long-term chromatic adaptation. Figure 2 shows the outline of our method.

The idea is that, we utilize the complementary pairs of the locally approximated color cast to modify the image colors, such that any image colors similar to the color cast are muted, while the others keep their differences relative to the color cast. In other words, we shift the reference color from the chromatic color cast, typically blue and green, to a neutral gray. The resulted color distribution has softer contrast and lower saturation due to the long-term adaptation. Hence, for visualization purposes, we enhance the image while preserving the adapted hues.

In particular, we consider the CIELAB color space and formulate the CAT adaptation process as a Tikhonov-type optimization problem [37]. As a metric space, CIELAB is a subspace of the three dimensional Euclidean space, where the distance between any two colors measures their perceptive difference. Using the CIELAB color difference metric, our optimization model consists of a fidelity term and a regularization characterizing the behavior of CAT adaptation. Then we enhance the adapted color distribution for visualization purposes. We also address some technical issues about CIELAB to improve its uniformity. These modifications are kept minimal so that problematic behaviors are effectively adjusted, and high efficiency is achieved.

To summarize, our contributions in this paper are:

1. We propose a novel approach for underwater image color correction using a Tikhonov-type optimization model in CIELAB color space.
2. We present a new mathematical interpretation of the complementary adaptation theory by Gibson for the color constancy of HVS.

3. We design a simple procedure to effectively improve the uniformity of CIELAB.

We organize this paper as follows. In Section 2, we present in detail our proposed method. In Section 3, we conduct various numerical experiments to analyze the model’s behaviors and quantitatively compare our method with some state-of-art techniques based on underwater-specific image quality metrics. We conclude the paper in Section 4 and include some technical details in the Appendix.

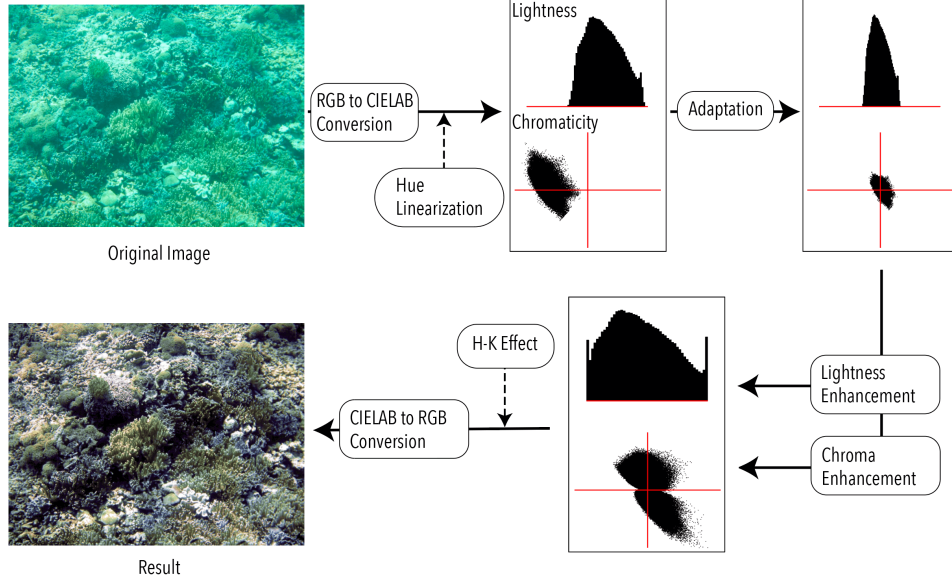


Figure 2: Pipeline of the proposed method. The result shown here uses  $\eta = 10, \beta = 1/3$  as the model parameters.

## 2 Proposed Method

### 2.1 Notations

Before stating our model, we fix some notations. We denote an arbitrary color by  $\mathbf{c}$ , which is specified in the CIELAB color space by its lightness  $L^*$ , red-green value:  $a^*$ , and yellow-blue value:  $b^*$ , i.e.,  $\mathbf{c} = (L^*, a^*, b^*)$ . In particular, the range for  $L^*$  is  $[0, 100]$ , where  $L^* = 0$  yields black and  $L^* = 100$  yields diffuse white. The  $a^*$ - $b^*$  section specifies the chromaticity. A positive value of  $a^*$  indicates red while a negative value gives green. A positive value of  $b^*$  indicates yellow and a negative value gives blue. From CIELAB, one can derive

$$\text{Chroma: } C^* = \sqrt{(a^*)^2 + (b^*)^2}, \quad (1)$$

which measures the relative saturation of  $\mathbf{c}$ , and

$$\text{Hue angle: } h^\circ = \text{atan2}(b^*, a^*), \quad (2)$$

which defines the hue of  $\mathbf{c}$ .

Given a pair of colors  $\mathbf{c}_i = (L_i^*, a_i^*, b_i^*)$ ,  $i = 1, 2$ , the CIELAB color difference between them is computed by

$$\Delta E^*(\mathbf{c}_1, \mathbf{c}_2) = \sqrt{(L_1^* - L_2^*)^2 + (a_1^* - a_2^*)^2 + (b_1^* - b_2^*)^2}, \quad (3)$$

which is simply the Euclidean distance between the CIELAB coordinates of the colors to be compared. This formula suggests that CIELAB color space is designed to be uniform.

The complementary color of  $\mathbf{c}$  in CIELAB is denoted by  $\mathbf{c}^-$ , which is computed by

$$\mathbf{c}^- = (100 - L^*, -a^*, -b^*) . \quad (4)$$

On a rectangular image domain  $\Omega = [0, W] \times [0, H] \subset \mathbb{R}^2$ ,  $W, H > 0$ , we define a color image, or a color distribution as a mapping  $\mathbf{c}$  from  $\Omega$  to the CIELAB color space

$$\mathbf{c}(x, y) = (L^*(x, y), a^*(x, y), b^*(x, y)) , \quad (x, y) \in \Omega . \quad (5)$$

For a triplet  $\sigma = (\sigma_1, \sigma_2, \sigma_3) \in \mathbb{R}^3$  with positive entries, we define the component-wise Gaussian convolution  $\mathcal{G}_\sigma$  applied on a color distribution  $\mathbf{c}$  as

$$\mathcal{G}_\sigma * \mathbf{c}(x, y) = (\mathcal{G}_{\sigma_1} * L^*(x, y), \mathcal{G}_{\sigma_2} * a^*(x, y), \mathcal{G}_{\sigma_3} * b^*(x, y)) , \quad (6)$$

where each component is the ordinary Gaussian convolution with intensity specified by  $\sigma_i$ ,  $i = 1, 2, 3$ . We take mirror reflect for computing the convolved values near the image boundary.

## 2.2 Complementary Adaptation Model in CIELAB

Given a color distribution  $\mathbf{c}_0 = (L_0^*, a_0^*, b_0^*)$  over  $\Omega$ , we propose the **Complementary Adaptation Model** by defining the adapted color at  $(x, y) \in \Omega$  as the minimizer of the following optimization problem

$$\mathbf{c}_{\text{adapt}}(x, y) = \arg \min_{\mathbf{c} \in \mathbb{R}^3} (\Delta E^*(\mathbf{c}(x, y), \mathbf{c}_0(x, y)))^2 + \lambda (\Delta E^*(\mathbf{c}(x, y), (\mathcal{G}_\sigma * \mathbf{c}_0(x, y))^-))^2 , \quad (7)$$

where  $\lambda > 0$  is a weight parameter, and  $\sigma = (\sigma_{L^*}, \sigma_{a^*}, \sigma_{b^*})$  such that  $\sigma_{a^*} = \sigma_{b^*}$  and  $\sigma_{L^*} = n\sigma_{a^*}$  for some  $n > 1$ . This is a Tikhonov-type optimization problem consisting of two terms. The first term measures the difference between the given color distribution  $\mathbf{c}_0$  and the adapted color  $\mathbf{c}_{\text{adapt}}$ , thus it imposes the fidelity condition. The second term models the effect of CAT adaptation process, which acts as a regularization. The proposed color distribution  $\mathbf{c}_{\text{adapt}}$  is a balance between the original image and the complementary of the estimated color cast  $\mathcal{G}_\sigma * \mathbf{c}$ . In this paper, we fix  $\sigma_{a^*} = \sigma_{b^*} = \sigma_0 := 0.25(\max(W, H)/2 - 1)$  so that the size of the filter is roughly  $\max(W, H)/2$ ,  $n = 3$ , and  $\lambda = 1$ .

Thanks to the simple formula (3) for computing the color difference, (7) has a unique global minimizer obtained by calculus:

$$\mathbf{c}_{\text{adapt}}(x, y) = (L_{\text{adapt}}^*(x, y), a_{\text{adapt}}^*(x, y), b_{\text{adapt}}^*(x, y)) , \quad (8)$$

where

$$\begin{cases} L_{\text{adapt}}^*(x, y) = (L_0^*(x, y) + (100 - \mathcal{G}_{3\sigma_0} * L_0^*(x, y))) / 2 \\ a_{\text{adapt}}^*(x, y) = (a_0^*(x, y) - \mathcal{G}_{\sigma_0} * a_0^*(x, y)) / 2 \\ b_{\text{adapt}}^*(x, y) = (b_0^*(x, y) - \mathcal{G}_{\sigma_0} * b_0^*(x, y)) / 2 \end{cases} \quad (9)$$

This formulation shows that the adapted color  $\mathbf{c}_{\text{adapt}}(x, y)$  is the midpoint of the image color  $\mathbf{c}_0(x, y)$  and the complementary pair of the estimated color cast at  $(x, y)$  in the CIELAB space.

Some remarks are needed for the proposed model:

1. *Locality principle*: The adaptation is spatially dependent [24]. Notice that in the second term of the model, the complementary operator is applied to the Gaussian filtered color distribution instead of the original  $\mathbf{c}_0$ . The locality of the adaptation is adjusted by the parameter  $\sigma_0$ . A greater value of  $\sigma_0$  implies a larger field of adaptation and the estimated color cast is spatially more uniform. In contrast, a smaller value of  $\sigma_0$  induces a more focused adaptation and the estimated color cast is more variant. Consequently, the neutralization effect is stronger when  $\sigma_0$  is small; when  $\sigma_0 \rightarrow 0$ , the adapted color distribution becomes uniformly neutral gray.

2. *CIELAB gamut consideration*: In practice, the 3-tuple  $\mathbf{c}_{\text{adapt}}$  computed by (9) stay inside the CIELAB gamut. There are two reasons to support this statement. First, the adapted lightness  $L_{\text{adapt}}^*$  concentrates around 50, where the chromaticity section of the CIELAB gamut has the most extended domain (Figure 12 (a) and (b)). Second, the dominating color casts in underwater images are mostly blue or green. Observe that the CIELAB gamut (Figure 12 (c)) corresponding to the green-blue region only has limited expansion, hence both  $\mathcal{G}_{\sigma_0} * a_0^*$  and  $\mathcal{G}_{\sigma_0} * b_0^*$  are relatively small. Consequently, the triangle spanned by  $(a_0^*, b_0^*)$  and  $(\mathcal{G}_{\sigma_0} * a_0^*, \mathcal{G}_{\sigma_0} * b_0^*)$  is most likely contained in the chromaticity domain at the lightness  $L_{\text{adapt}}^*$ . For robustness, in case  $\mathbf{c}_{\text{adapt}}(x, y)$  for some  $(x, y)$  falls outside the CIELAB gamut, we keep its adapted lightness and hue angle while shrinking its chroma to the corresponding maximal chroma. Other possible solutions can be found in [1] and [39].
3. *Long-term adaptation*: The proposed color distribution  $\mathbf{c}_{\text{adapt}}$  is based on the neutralization of dominant colors, which is a long-term chromatic adaptation that can take multiple days [3, 38]. This is different from the daily experience where the time of adaptation ranges from seconds to a few minutes [35]. Similarly to the experimental setting [3], the Gaussian filtered color distribution can be considered as colored lenses, and the long-term adaptation behavior is modeled by the regularization term. Hence, our model predicts the perceived colors when the observer wears the lenses for a long time and the dominant colors are neutralized by their complementary pairs, respectively.
4. *Connection to other works*: The proposed model (7) also provides a variational substitute for the well-known Gray World (GW) assumption [8], which is a key component in many methods in the literature, e.g., ACE [6]. In [6], Bertalmio et al. connect ACE to the Wilson-Cowan equations [41] from computational neuroscience, where the GW assumption is used to set an absolute neutral state such that only deviations from this level are considered meaningful. Noticing the drawback of using an absolute level, in [5], Bertalmio proposes to replace it with a local average; however, by doing so, no color correction is in action. Our model provides an elegant solution which maintains an effective color correction while avoiding an absolute reference.

### 2.3 Robust Hue-preserving Image Enhancement

The adapted color distribution  $\mathbf{c}_{\text{adapt}}$  represents a long-term result rarely achieved in common life experience. For visualization purpose, we enhance the lightness  $L_{\text{adapt}}^*$  and the chroma  $C_{\text{adapt}}^*$  (1) computed using  $a_{\text{adapt}}^*$ ,  $b_{\text{adapt}}^*$ , while preserving the adapted hue  $h_{\text{adapt}}^\circ$  (2) where the dominant color cast has been neutralized.

We enhance the adapted lightness by a linear stretch. The enhanced lightness is denoted by  $\widehat{L}_{\text{adapt}}^*$ . To keep the transform consistent with the CIELAB gamut, we rescale the chroma of the adapted colors by

$$C_1^*(x, y) = \left( \frac{C_{\text{adapt}}^*(x, y)}{C_{\text{max}}^*(L_{\text{adapt}}^*(x, y), h_{\text{adapt}}^\circ(x, y))} \right) \times C_{\text{max}}^*(\widehat{L}_{\text{adapt}}^*(x, y), h_{\text{adapt}}^\circ(x, y)). \quad (10)$$

which preserves the percentage of the relative saturation of  $\mathbf{c}_{\text{adapt}}$ . Here  $C_{\text{max}}^*(L^*, h^\circ)$  denotes the maximal chroma in the CIELAB gamut when the lightness is  $L^*$  and the hue angle is  $h^\circ$ , whose computation is detailed in the Appendix A. Notice that the adapted hue angles are unchanged during this rescaling.

For the fixed lightness  $\widehat{L}_{\text{adapt}}^*$ , we enhance the chroma of the newly obtained color distribution  $(\widehat{L}_{\text{adapt}}^*, a_1^*, b_1^*)$  by the following transformation

$$C_2^*(x, y) = \left( \frac{C_1^*(x, y)}{C_{\text{max}}^*(\widehat{L}_{\text{adapt}}^*(x, y), h_{\text{adapt}}^\circ(x, y))} \right)^{1/\eta} \times C_{\text{max}}^*(\widehat{L}_{\text{adapt}}^*(x, y), h_{\text{adapt}}^\circ(x, y)). \quad (11)$$



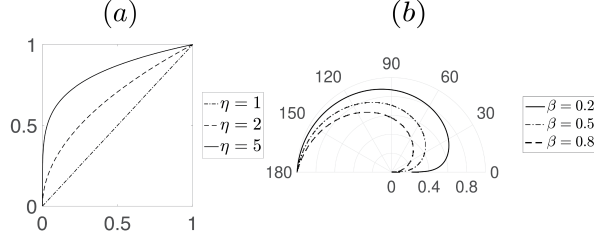


Figure 3: (a) Gamma function used for chroma enhancement (11) with varying values of  $\eta$ . (b) Robust factor (12) for suppressing the noisy hues with varying values of  $\beta$ .

We note that this is a gamma correction applied to the percentage of relative saturation. See Figure 3 (a). Here,  $\eta \geq 1$  is the enhancing parameter. When  $\eta$  increases, a stronger enhancement is applied, and when  $\eta = 1$ , the gamma function reduces to the identity map.

To improve stability, for some  $0 < \beta \leq 1$ , we define

$$\text{Robust factor: } F(\theta) = \left(\frac{\theta}{180^\circ}\right)^\beta, \quad (12)$$

for any  $\theta \in [0, 180^\circ]$ ,

whose behavior is shown in Figure 3 (b). We propose the robust hue-preserving enhancement of the adapted color distribution  $\mathbf{c}_{\text{adapt}}$  by

$$\widehat{\mathbf{c}}_{\text{adapt}}(x, y) = (\widehat{L}^*_{\text{adapt}}(x, y), \widehat{a}^*_{\text{adapt}}(x, y), \widehat{b}^*_{\text{adapt}}(x, y)), \quad (13)$$

where

$$\begin{cases} \widehat{a}^*_{\text{adapt}}(x, y) = F(\theta(x, y))a_2^*(x, y) \\ \widehat{b}^*_{\text{adapt}}(x, y) = F(\theta(x, y))b_2^*(x, y) \end{cases}. \quad (14)$$

and  $\theta(x, y)$  denotes the hue angle difference between the image color and the estimated color cast at  $(x, y)$ . Notice that by multiplying the robust factor, when  $\theta(x, y) \approx 0^\circ$ , i.e., the hue angle difference between the image color and the estimated color cast is small,  $\widehat{\mathbf{c}}_{\text{adapt}}(x, y)$  becomes almost achromatic. As for image colors deviating from the estimated color cast at the same locations, the differences are emphasized.

## 2.4 Improvement on the Uniformity of CIELAB

The main purpose of the CIELAB as an alternative to RGB is to quantify the perceptive color difference. This is only approximate due to the intrinsic complexity and non-linearity of the HVS. In this work, we employ two simple modifications to achieve a better uniformity.

### 2.4.1 Adjustment in the Blue Region

As known to many researchers [7, 10, 25, 29], the blue region of CIELAB, which roughly corresponds to the subset of colors with hue angles ranging from  $250^\circ$  to  $300^\circ$ , is not hue-linear. It means that, with the CIELAB lightness and hue angle fixed, increasing the CIELAB chroma yields a perceivable hue-shift.

In this work, we propose to address this technical problem by applying the following transform before solving for the adapted color distribution via (7):

$$h_{\text{adjust}}^\circ = h^\circ - \mu^\circ \times \sqrt{\frac{(C^*)^m}{(C^*)^m + 10^m}} \times \exp\left(-\left(\frac{h^\circ - 275^\circ}{25^\circ}\right)^2\right). \quad (15)$$

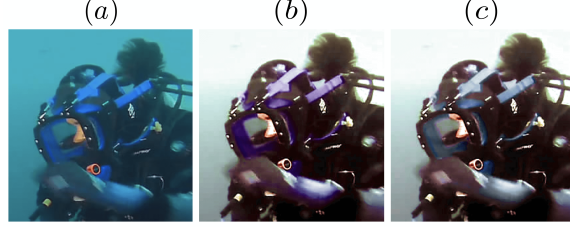


Figure 4: Pre-processing by hue angle adjustment in the blue region of CIELAB. (a) Part of an underwater image. (b) Proposed method without the pre-processing (15). (c) Proposed method with the pre-processing. With the adjustment, the blueness on the strap is preserved.

This formula is modified from [23], which adjusts the hue angle by a product of three factors. The first factor  $\mu^\circ$  denotes the maximal distorted hue angle. The second factor predicts the increase of the hue rotation from neutral, i.e.,  $C^* = 0$  until around  $C^* = 10$  and remains constant in the high chroma region [23]. The last factor restricts the hue adjustment within the region  $275^\circ < h^\circ < 300^\circ$ . We fix  $\mu^\circ = 45^\circ$  and choose  $m = 7$  in this paper. For a more precise hue adjustment based on a look-up-table, we refer the readers to [7].

For underwater images, the pre-processing (15) is especially important, since the general color distributions concentrate around the blue region. In Figure 4, we apply the proposed method to an underwater image (a) without the hue adjustment (15) and the blue goggle straps turn into purple (b). With the hue correction (c), we observe that the blueness is correctly preserved. Hence, including the adjustment (15) as a pre-processing compensates for the distortion of the hue angle as we enhance the chroma.

#### 2.4.2 The Helmholtz-Kohlrausch Effect

The Helmholtz-Kohlrausch (H-K) effect is a perceptual phenomenon where the perceived lightness of a color with increasing saturation is brighter [9]. To enhance the chroma (14) while keeping the perceived lightness unchanged, we need to adjust  $\widehat{L}_{\text{adapt}}^*$ . For an arbitrary color  $\mathbf{c} = (L^*, a^*, b^*)$  in CIELAB, the perceived lightness  $L_{\text{H-K}}^*$  when considering the H-K effect can be estimated by [11]

$$L_{\text{H-K}}^* = L^* + (2.5 - 0.025L^*)g(h^\circ)C^*, \quad (16)$$

where

$$g(h^\circ) = 0.116 \times \left| \sin \left( \frac{h^\circ - 90^\circ}{2} \right) \right| + 0.085. \quad (17)$$

$$(18)$$

Hence, assuming that  $\widehat{L}_{\text{adapt}}^*$  corresponds to the perceived lightness before the chroma enhancement, the associated CIELAB lightness after the chroma enhancement is computed by inverting (16), which gives

$$(\widehat{L}_{\text{adapt}}^*)_{\text{adjust}} = \frac{\widehat{L}_{\text{adapt}}^* - 2.5g(\widehat{h}_{\text{adapt}}^\circ)\widehat{C}_{\text{adapt}}^*}{1 - 0.025g(\widehat{h}_{\text{adapt}}^\circ)\widehat{C}_{\text{adapt}}^*}. \quad (19)$$

Similar improvement is also considered in [39] for food image enhancement.

The post-processing in regard to the HK-effect (16) addresses the over-exposure caused by the enhancing saturation. In Figure 5, we focus on a zoomed-in region of an underwater image (a) and show the result without the post-processing (b) as well as the processed one (c). Comparing these results, we observe that when the HK-effect is considered, the image contrast is also improved. See the patterns on the shorts and the red tube.

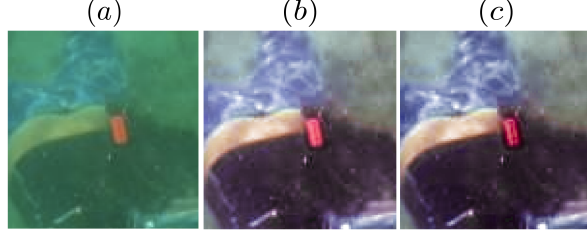


Figure 5: Post-processing considering the HK-effect. (a) Zoom-in of part of the underwater image in Figure 1. (b) Proposed method without the post-processing (16). (c) Proposed method with the post-processing. Post-processing considering the HK-effect reduces over-exposure.

### 3 Numerical Results

#### 3.1 General Examples

The proposed method is flexible and adaptive to different image contents. It yields improvements on the image contrasts and color balance which are typically degraded in underwater images. In Figure 6, we demonstrate various examples where underwater images are used for (a) submarine biology, (c) recreational purposes, and (e) field exploration. Given possible differences in the imaging environment and devices, our method shows consistent and stable behaviors in terms of removing the color casts and enhancing the image quality, and the corresponding processed results are in (b), (d), and (f).

#### 3.2 Different Underwater Color Cast

Underwater imaging environment is complicated and various conditions can affect the chromatic attributes of the color cast. In Figure 7, we show the stability of our proposed method for underwater images with different color casts. The scene in the first row shows strong blue veiling light (hue angles concentrating around  $210^\circ$ ), the one in the second row has a yellow color cast (around  $95^\circ$ ), and the third is dominated by a green color (around  $150^\circ$ ). In the third column, we observe that the hue angles of the processed results are more spread out, and the resulted images are displayed in the last row. Although the color casts in the original images are distinct, the colors different from the estimated color casts are preserved and emphasized in the final results.

#### 3.3 Necessity of the Robust Factor

The procedure (11) enhances the residual colors after the dominating cast is neutralized. Specifically, the absolute change of the hue angle can be expressed as

$$|h_{\text{adapt}}^\circ(x, y) - h_0^\circ(x, y)| = \frac{180^\circ}{\pi} \arccos \left( \frac{a_{\text{adapt}}^*(x, y)a_0^*(x, y) + b_{\text{adapt}}^*(x, y)b_0^*(x, y)}{C_{\text{adapt}}^*(x, y)C_0^*(x, y)} \right). \quad (20)$$

Let  $C_{\mathcal{G}}^*(x, y) = \sqrt{(\mathcal{G}_{\sigma_0} * a_0^*(x, y))^2 + (\mathcal{G}_{\sigma_0} * b_0^*(x, y))^2}$  be the chroma of the estimated color cast at  $(x, y)$ ,  $\rho(x, y) = C_0^*(x, y)/C_{\mathcal{G}}^*(x, y)$  as the ratio of image chroma and color cast chroma, and  $\gamma(x, y) = (a_0^*(x, y)(\mathcal{G}_{\sigma} * a_0^*)(x, y) + b_0^*(x, y)(\mathcal{G}_{\sigma} * b_0^*)(x, y))/(C_0^*(x, y)C_{\mathcal{G}}^*(x, y))$  as a measure of the hue angle difference between the image color and the color cast, then (20) can be rewritten as

$$\frac{180^\circ}{\pi} \arccos \left( \frac{\rho(x, y) - \gamma(x, y)}{\sqrt{\rho^2(x, y) - 2\gamma(x, y)\rho(x, y) + 1}} \right). \quad (21)$$

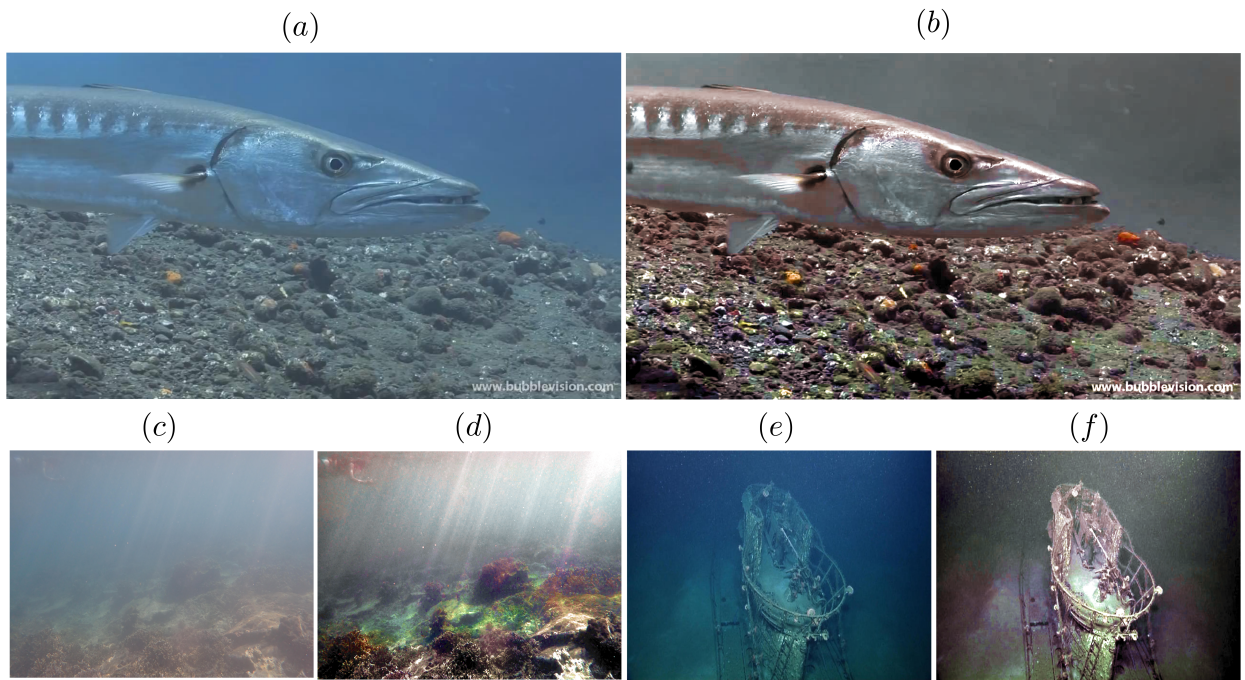


Figure 6: General examples of the proposed method. (a) A typical underwater image showing dominating blue cast, and the contrast is relatively low. (b) Result of the proposed method applied to (a) removes the blue cast and enhances the textures on the riverbed. (c) A blurry underwater image where objects are hardly visible. (d) Result of the proposed method applied to (c) which shows vibrant colors and sharp objects' boundaries. (e) A deep underwater image commonly seen in field exploration. (f) Result of the proposed method applied to (e) which renders the details of the structure of interest.



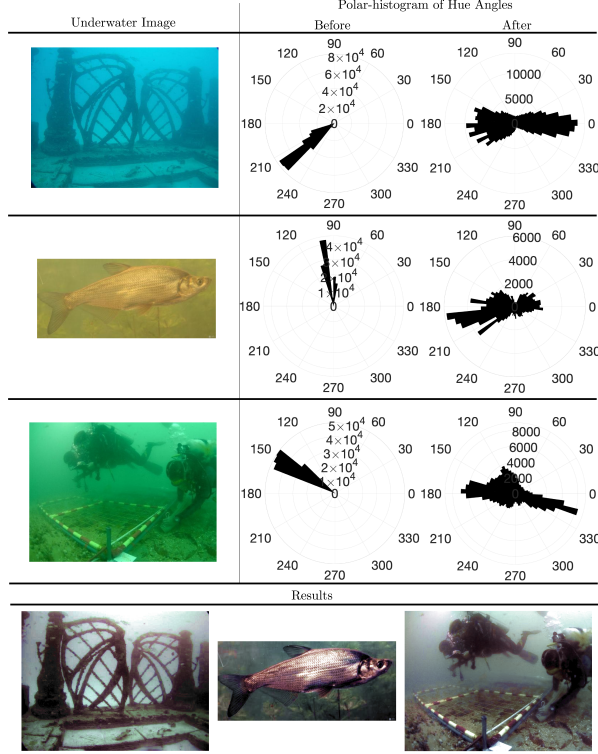


Figure 7: The proposed method shows consistent performance for underwater images with different color casts. For each underwater image in the first 3 rows, we show their hue angle distributions in the second column; in the third columns we show the distribution of the final results, which are displayed in the last row. In all cases, we have  $\eta = 6$  and  $\beta = 1/4$ .

Notice that when the image color and the estimated color cast have similar hue angles, i.e.,  $\gamma(x, y) \approx 1$ , (21) shows that

$$|h_{\text{adapt}}^{\circ}(x, y) - h_0^{\circ}(x, y)| \approx \begin{cases} 180^{\circ}, & \text{if } \rho(x, y) < 1 \\ 90^{\circ}, & \text{if } \rho(x, y) = 1 \\ 0^{\circ}, & \text{if } \rho(x, y) > 1 \end{cases}, \quad (22)$$

which is independent of the lightness. This implies that a direct enhancement as in (11) is very sensitive to the ratio of the image chroma and color cast chroma.

Such instability will cause chromatic noise in areas where the colors are slightly different from the estimated color cast, and typically this happens when the underwater image contains a large portion of background, e.g., Figure 8 (a). In Figure 8 (b), we show the image resulted from the direct enhancing (11) using  $\eta = 8$ , which presents noisy colors in the background region. A possible remedy is to use smaller values of  $\eta$ , however, this will also subdue the saturation of regions which deserve enhancing. For example, in Figure 8 (c) where we use  $\eta = 2$ , although the noisy colors in the background are suppressed, the riverbed becomes almost achromatic. By using the proposed robust factor (12), the corrected image as shown in Figure 8 (d) reduces the noise while maintaining a more saturated rendering outside the background region.

### 3.4 Behaviors of the Saturation Parameter $\eta$

The chroma enhancement parameter  $\eta$  (11) allows flexible adjustment of the image saturation. In Figure 9, fixing  $\beta = 1/3$ , we apply the proposed method to the underwater image (a) using  $\eta = 2$ ,  $\eta = 4$  and  $\eta = 10$ , which are shown in (b), (d), and (d), respectively. When we increase the parameter  $\eta$ , the saturated green color cast in the original image keeps muted, as it is

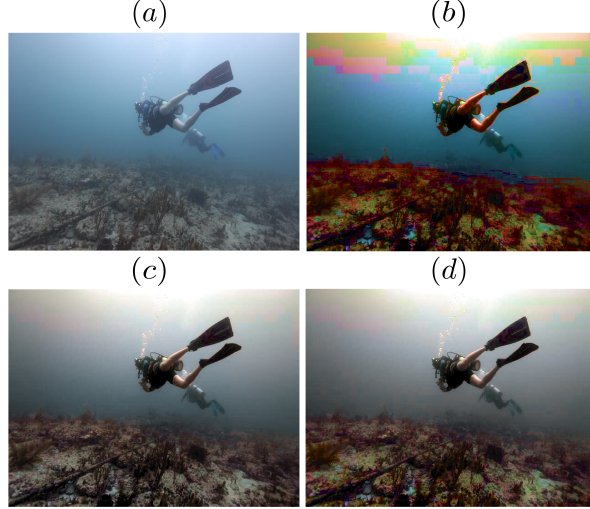


Figure 8: (a) Original underwater image. (b) Proposed method without applying the robust factor (12) ( $\eta = 8$ ). (c) Proposed method without applying the robust factor ( $\eta = 2$ ). (d) Proposed method with the robust factor ( $\eta = 8, \beta = 1/3$ ). Using the robust factor suppresses the background noisy colors while enhancing the saturation of the other regions.

neutralized before the chroma enhancement. As for the objects of colors different from the color cast, e.g., the string and statue, they become more recognizable when greater values of  $\eta$  are applied. This example demonstrates two features of our method.

First, objects of smaller scales compared to the radius of the Gaussian kernel used in (7) are the most distinguishable in the results. This is due to the fact that, the pixels of these objects have little impact on the estimated color cast, thus the complimentary pairs of the objects' colors will not contribute to the neutralization process according to CAT. Consequently, they preserve most of their chromatic properties and get emphasized after the neutralization of the color cast and the chroma enhancement. For instance, see the red string, the white oxymeter, and the texture of the sand.

Second, although enhancing the saturation by (11) is global, the background color remain relatively muted compared to others during this process. When we increase the value of  $\eta$ , the red string and brown statue become more saturated than the green background. This can render the objects in the scene more distinguishable and help improve the image contrast in a global scale.

### 3.5 Qualitative Comparison

We compare our proposed method to some of the state-of-art approaches in the literature. They are designed either specifically for underwater images, or for color constancy for general color images. On the original image in Figure 10 (a), we compare Zhao et al. [44] (shown in (b)), Peng et al. [31] (shown in (c)), Histogram Equalization (shown in (d)), Limare et al. [22] (shown in (e)), Automatic Color Correction (ACE) [6, 14], Local Color Correction [16] (shown in (g)), Multiscale Retinex [32, 34] (shown in (h)), and the proposed method in (i). We see that these methods exhibit different chromatic properties in their results.

Both (b) and (c) are obtained from underwater-image-specific approaches based on the Koschmieder model. They differ from each other by the techniques used for background light and transmission map estimation. As pointed out in [31], these estimated quantities determine the results, and in many cases, such relation is very sensitive. With careful combination of different priors and estimations, the result in (c) shows better color restoration on some region of the statue and the riverbed compared to (b).

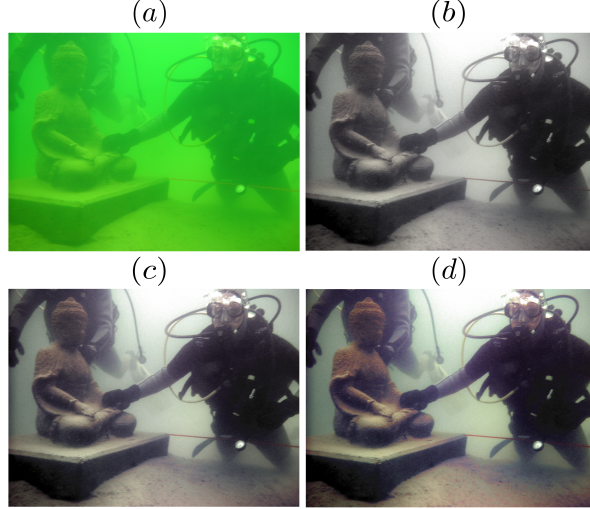


Figure 9: Effect of the chroma enhancement parameter  $\eta$ . (a) Original underwater image. (b) Result with  $\eta = 2$ . (c)  $\eta = 4$ . (d)  $\eta = 10$ . Here we fix  $\beta = 1/4$ .

The methods used in the second row manipulate the image histogram. For (d), we see the typical over-saturation in HE. The method in (e), which aims at enhancing the dynamical ranges of the RGB-channels, does not show effective color balancing in this example. As a localized version of HE, (f) renders more realistic colors compared to (d).

The method for (g) is based on a nonlinear filter applied in the HSL color space, which demonstrate enhancement on the brightness and saturation, yet the green cast is not removed. The Multiscale Retinex used in (h) improves the image brightness and makes many textures visible, but the colors are still biased toward green.

The proposed method in (i) shows distinct visual perception from the others. First, the strong green cast in the original underwater image is effectively removed. This renders a neutral background and recovers realistic tones for the statue, which is perceived as white in (a). Second, the colors for small-scale textures become apparent. For example, we clearly see the brownish mud around the statue and the color variations on the riverbed. Third, because of the neutralization of the background and the enhancement on the small scale contents, our result shows better contrast improvement. Notice the head and shoulder of the statue, as well as the patterns on the pottery.

### 3.6 Quantitative Evaluation and Comparison

In this set of experiments, we evaluate the performances of the proposed algorithm and other methods in the literature using two measures: Underwater Color Image Quality Evaluation metric (UCIQE) [42] and Underwater Image Quality Measure (UIQM) [30]. These metrics are specifically designed to evaluate the quality of underwater images. Both UCIQE and UIQM are linear combinations of certain image attributes such as colorfulness, saturation, and contrast, whose coefficients are statistically derived. Higher values of these metrics indicate better image qualities.

Figure 11 collectively shows the results from Histogram Equalization, Peng et al. [31], Automatic Color Enhancement (ACE) [6], and the proposed method, where the underwater images have various contents and complexities. Our method performs consistently the best measured by UIQM, and the values of UICQE for some of our results are the highest. Among all the methods in comparison, HE produces the most colorful results, yet some of which are overly saturated. The method proposed by Peng et al. performs well when the veiling light color is correctly estimated. ACE is a local HE in principle, hence we observe similar chromatic features





Figure 10: Qualitative comparison of different methods for underwater images. (a) Original underwater image. (b) Zhao et al. [44] (c) Peng et al. [31] (d) Histogram Equalization (HE) (e) Limare et al. [22] (f) Automatic Color Enhancement (ACE) [6,14] (g) Local Color Correction [16] (h) Multiscale Retinex [32,34] (i) Proposed Method. Our method has distinct characteristics compared to the others: effective color cast removal, prominent enhancement on the colors of small-scale textures, and sharp objects' boundaries.



between them. Compared to HE, ACE produces more natural color distributions. Among the results from the proposed method, observe that a common characteristic is that the strong color casts in the original underwater images are neutralized. This feature induces a visual effect that the objects against the original saturated background have sharper boundaries.

## 4 Conclusion

In this paper, we presented a new mathematical interpretation of the complimentary adaptation theory proposed by Gibson in 1937. As an alternative of the well-known Retinex theory for understanding the color constancy, CAT emphasizes the neutralization function of the complementary pair of the lasting stimulus rather than HVS's competence of identifying the reflectance. We modeled this adaptation process as a Tikhonov-type optimization problem in the CIELAB color space. This is a simple model which produces the adapted colors as a balance between the original underwater image and the complimentary pair of the estimated color cast. We overcame the lack of uniformity of CIELAB by employing two techniques: a pre-processing compensating the hue-distortion in the blue region, and a post-processing addressing the H-K effect. Numerically, we demonstrated the necessities of the introduced techniques and qualitatively compared our model with some of the state-of-art methods for underwater images. The proposed method shows superior stability when dealing with various underwater environments and recovers realistic colors compatible with the visual perception.

## A CIELAB Boundary Estimation

The RGB color space is geometrically a cube embedded in the Euclidean space  $\mathbb{R}^3$ , however, the transformation from RGB to CIELAB maps the RGB cube to an irregular shape. See the illustration in Figure 12 (a)–(c). Here, we randomly sample 500000 points in the RGB cube, convert them to the CIELAB space, digitize their lightness coordinates by taking the ceil function, and compute the convex hull of the chromaticity section for each digitized lightness. Hence, the CIELAB gamut is approximated by the union of these convex slices at different lightness levels

$$\bigcup_{L^*=0}^{100} \text{conv}\{V_i(L^*)\}_{i=1}^{N(L^*)}, \quad (23)$$

where  $V_i(L^*)$  represents a vertex of the convex hull computed using the color samples with digitized lightness  $L^*$ , and  $\text{conv}\{\cdot\}$  computes the convex hull supported by a finite set of points. This approach offers a simple estimation of the chroma boundary given the lightness  $L^*$  and hue angle  $h^\circ$  according to basic trigonometry

$$C_{\max}^*(L^*, h^\circ) = \frac{l_{j(h^\circ)} \sin(\rho_{j(h^\circ)})}{\sin(\pi - \theta_{j(h^\circ)} - \rho_{j(h^\circ)})}, \quad (24)$$

$$j(h^\circ) \in \{1, 2, \dots, N(L^*)\}$$

where  $\theta_{j(h^\circ)} < h^\circ < \theta_{j(h^\circ)+1}$ ,  $\theta_{j(h^\circ)}$  is the angle from the positive direction of the  $a^*$ -axis to  $V_{j(h^\circ)}(L^*)$  in a counter-clockwise orientation,  $\theta_{N(L^*)+1}$  takes  $\theta_1$ , and  $l_{j(h^\circ)}$  is the distance from  $V_{j(h^\circ)}(L^*)$  to the origin. Both quantities  $l_{j(h^\circ)}$  and  $\theta_{j(h^\circ)}$  depend on  $L^*$ , and we suppress this notation in (24) for simplicity. See Figure 12 (d) for an illustration.

## Acknowledgment

The author would like to thank Professor Sung Ha Kang from School of Mathematics of Georgia Institute of Technology for valuable discussion and suggestions, and Dr. Chongyi Li from City

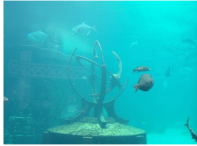









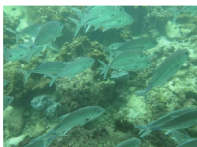


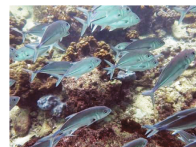
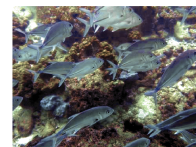

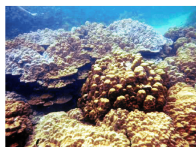


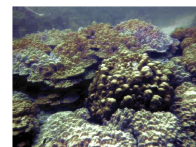





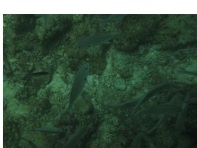
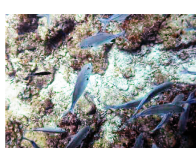
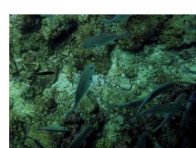
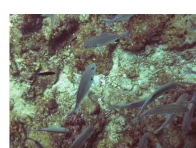

Underwater Image	HE		Peng et al.		ACE		Proposed	
								
15.4562 9.7401	34.7763 10.5910	20.6511 10.1054	28.0375 10.4630	31.2793 10.6749				
								
13.0788 9.4481	31.8792 10.4281	35.1049 10.1408	28.0321 10.2757	30.7094 10.5384				
								
13.6919 10.0128	30.2996 10.8710	22.2851 10.5369	29.4427 10.6661	31.3955 10.8797				
								
10.6763 9.6017	32.7145 10.8361	15.4660 10.1500	28.4755 10.5972	33.1036 10.8481				
								
8.2525 9.3383	31.5581 10.5508	19.6950 9.9460	24.2148 10.3023	29.2597 10.5969				
								
16.9022 10.0163	30.9155 10.8021	29.0229 10.6899	24.4996 10.6001	31.8314 10.8797				

Figure 11: Quantitative evaluation and comparison. We compare our methods with Histogram Equalization (HE), Peng et al. [31], and Automatic Color Enhancement (ACE) [6, 14]. The quality of each image is evaluated by UCIQE [42] (left, blue marks the best) and UIQM [30] (right, red marks the best). In all the cases, we use  $\eta = 10$  and  $\beta = 1/4$  for the proposed method.

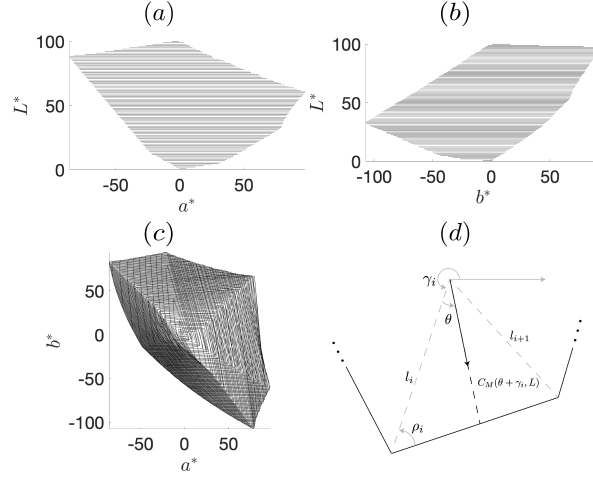


Figure 12: (a) CIELAB gamut projection on the  $L^*-a^*$  plane. (b) Projection on the  $L^*-b^*$  plane. (c) Projection on the  $a^*-b^*$  plane. (d) Geometry for computing the chroma upper limit  $C_{\max}^*(L, \theta + \gamma_i)$  in the direction of the hue angle  $\theta + \gamma_i$  on the lightness level of  $L$ . Here the chroma direction falls within the sector  $[\gamma_i, \gamma_{i+1}]$ ,  $i = 1, 2, \dots$

University of Hong Kong for sharing the data set of underwater images used in this paper.

## References

- [1] Tadahiro Azetsu and Noriaki Suetake. Hue-preserving image enhancement in CIELAB color space considering color gamut. *Optical Review*, 26(2):283–294, 2019.
- [2] Jacob Beck. The perception of surface color. *Scientific American*, 233(2):62–77, 1975.
- [3] Suzanne C Belmore and Steven K Shevell. Very-long-term and short-term chromatic adaptation: are their influences cumulative? *Vision research*, 51(3):362–366, 2011.
- [4] Dana Berman, Tali Treibitz, and Shai Avidan. Diving into haze-lines: Color restoration of underwater images. In *Proc. British Machine Vision Conference (BMVC)*, volume 1, 2017.
- [5] Marcelo Bertalmío. From image processing to computational neuroscience: a neural model based on histogram equalization. *Frontiers in computational neuroscience*, 8:71, 2014.
- [6] Marcelo Bertalmío, Vicent Caselles, Edoardo Provenzi, and Alessandro Rizzi. Perceptual color correction through variational techniques. *IEEE Transactions on Image Processing*, 16(4):1058–1072, 2007.
- [7] Gustav J Braun, Mark D Fairchild, and Fritz Ebner. Color gamut mapping in a hue-linearized CIELAB color space. In *Color and imaging conference*, volume 1998, pages 163–168. Society for Imaging Science and Technology, 1998.
- [8] Gershon Buchsbaum. A spatial processor model for object colour perception. *Journal of the Franklin institute*, 310(1):1–26, 1980.
- [9] Robert L Donofrio. The Helmholtz-Kohlrausch effect. *Journal of the Society for Information Display*, 19(10):658–664, 2011.
- [10] Fritz Ebner and Mark D Fairchild. Finding constant hue surfaces in color space. In *Color Imaging: Device-Independent Color, Color Hardcopy, and Graphic Arts III*, volume 3300, pages 107–117. International Society for Optics and Photonics, 1998.

- [11] Mark D Fairchild and Elizabeth Pirrotta. Predicting the lightness of chromatic object colors using CIELAB. *Color Research & Application*, 16(6):385–393, 1991.
- [12] Graham Finlayson and Steven Hordley. Improving gamut mapping color constancy. *IEEE Transactions on Image Processing*, 9(10):1774–1783, 2000.
- [13] Graham D Finlayson, Mark S Drew, and Brian V Funt. Spectral sharpening: sensor transformations for improved color constancy. *JOSA A*, 11(5):1553–1563, 1994.
- [14] Pascal Getreuer. Automatic Color Enhancement (ACE) and its Fast Implementation. *Image Processing On Line*, 2:266–277, 2012.
- [15] James J Gibson. Adaptation with negative after-effect. *Psychological review*, 44(3):222, 1937.
- [16] Juan Gabriel Gomila Salas and Jose Luis Lisani. Local Color Correction. *Image Processing On Line*, 1:260–280, 2011.
- [17] N Jerlov. Irradiance optical classification. *Optical Oceanography*, pages 118–120, 1968.
- [18] Ron Kimmel, Michael Elad, Doron Shaked, Renato Keshet, and Irwin Sobel. A variational framework for retinex. *International Journal of computer vision*, 52(1):7–23, 2003.
- [19] Harald Koschmieder. Theorie der horizontalen sichtweite. *Beitrage zur Physik der freien Atmosphäre*, pages 33–53, 1924.
- [20] Edwin H Land. The retinex theory of color vision. *Scientific american*, 237(6):108–129, 1977.
- [21] Chongyi Li, Chunle Guo, Wenqi Ren, Runmin Cong, Junhui Hou, Sam Kwong, and Dacheng Tao. An underwater image enhancement benchmark dataset and beyond. *IEEE Transactions on Image Processing*, 29:4376–4389, 2019.
- [22] Nicolas Limare, Jose-Luis Lisani, Jean-Michel Morel, Ana Belén Petro, and Catalina Sbert. Simplest Color Balance. *Image Processing On Line*, 1:297–315, 2011.
- [23] M Ronnier Luo, Guihua Cui, and Bryan Rigg. The development of the CIE 2000 colour-difference formula: CIEDE2000. *Color Research & Application: Endorsed by Inter-Society Color Council, The Colour Group (Great Britain), Canadian Society for Color, Color Science Association of Japan, Dutch Society for the Study of Color, The Swedish Colour Centre Foundation, Colour Society of Australia, Centre Français de la Couleur*, 26(5):340–350, 2001.
- [24] JJ McCann. Local/global mechanisms for color constancy. *Die Farbe*, 34:275–283, 1987.
- [25] K McLaren. CIELAB hue-angle anomalies at low tristimulus ratios. *Color Research & Application*, 5(3):139–143, 1980.
- [26] Andrew Moore, John Allman, and Rodney M Goodman. A real-time neural system for color constancy. *IEEE Transactions on Neural networks*, 2(2):237–247, 1991.
- [27] Jean-Michel Morel, Ana B Petro, and Catalina Sbert. Fast implementation of color constancy algorithms. In *Color Imaging XIV: Displaying, Processing, Hardcopy, and Applications*, volume 7241, page 724106. International Society for Optics and Photonics, 2009.
- [28] Jean Michel Morel, Ana Belén Petro, and Catalina Sbert. A PDE formalization of retinex theory. *IEEE Transactions on Image Processing*, 19(11):2825–2837, 2010.



- [29] Nathan Moroney. A hypothesis regarding the poor blue constancy of CIELAB. *Color Research & Application: Endorsed by Inter-Society Color Council, The Colour Group (Great Britain), Canadian Society for Color, Color Science Association of Japan, Dutch Society for the Study of Color, The Swedish Colour Centre Foundation, Colour Society of Australia, Centre Français de la Couleur*, 28(5):371–378, 2003.
- [30] Karen Panetta, Chen Gao, and Sos Agaian. Human-visual-system-inspired underwater image quality measures. *IEEE Journal of Oceanic Engineering*, 41(3):541–551, 2016.
- [31] Yan-Tsung Peng and Pamela C Cosman. Underwater image restoration based on image blurriness and light absorption. *IEEE transactions on image processing*, 26(4):1579–1594, 2017.
- [32] Ana Belén Petro, Catalina Sbert, and Jean-Michel Morel. Multiscale Retinex. *Image Processing On Line*, pages 71–88, 2014.
- [33] Edoardo Provenzi, Massimo Fierro, Alessandro Rizzi, Luca De Carli, Davide Gadia, and Daniele Marini. Random spray retinex: a new retinex implementation to investigate the local properties of the model. *IEEE Transactions on Image Processing*, 16(1):162–171, 2006.
- [34] Zia-ur Rahman, Daniel J Jobson, and Glenn A Woodell. Multi-scale retinex for color image enhancement. In *Proceedings of 3rd IEEE International Conference on Image Processing*, volume 3, pages 1003–1006. IEEE, 1996.
- [35] Steven K Shevell. The time course of chromatic adaptation. *Color Research & Application: Endorsed by Inter-Society Color Council, The Colour Group (Great Britain), Canadian Society for Color, Color Science Association of Japan, Dutch Society for the Study of Color, The Swedish Colour Centre Foundation, Colour Society of Australia, Centre Français de la Couleur*, 26(S1):S170–S173, 2001.
- [36] DF Swinehart. The Beer-Lambert law. *Journal of chemical education*, 39(7):333, 1962.
- [37] Andrei Nikolaevich Tikhonov. On the solution of ill-posed problems and the method of regularization. In *Doklady Akademii Nauk*, volume 151, pages 501–504. Russian Academy of Sciences, 1963.
- [38] Katherine EM Tregillus and Stephen A Engel. Long-term adaptation to color. *Current Opinion in Behavioral Sciences*, 30:116–121, 2019.
- [39] Chiaki Ueda, Tadahiro Azetsu, Noriaki Suetake, and Eiji Uchino. Lightness and chroma enhancement for food images considering helmholtz-kohlrausch effect. *Optical Review*, 24(3):301–309, 2017.
- [40] Haocheng Wen, Yonghong Tian, Tiejun Huang, and Wen Gao. Single underwater image enhancement with a new optical model. In *2013 IEEE International Symposium on Circuits and Systems (ISCAS2013)*, pages 753–756. IEEE, 2013.
- [41] Hugh R Wilson and Jack D Cowan. Excitatory and inhibitory interactions in localized populations of model neurons. *Biophysical journal*, 12(1):1–24, 1972.
- [42] Miao Yang and Arcot Sowmya. An underwater color image quality evaluation metric. *IEEE Transactions on Image Processing*, 24(12):6062–6071, 2015.
- [43] Kailin Zhang and Hailong Huang. Underwater image transmission and blurred image restoration. *Optical Engineering*, 40(6), 2001.

- [44] Xinwei Zhao, Tao Jin, and Song Qu. Deriving inherent optical properties from background color and underwater image enhancement. *Ocean Engineering*, 94(jan.15):163–172.
- [45] Dominique Zosso, Giang Tran, and Stanley J Osher. Non-local retinex—a unifying framework and beyond. *SIAM Journal on Imaging Sciences*, 8(2):787–826, 2015.